

Second-Harmonic Distortion in Vertical-Cavity Surface-Emitting Lasers with Lateral Loss Effects

P. C. Chui and S.-F. Yu

Abstract—The influence of lateral loss effects on the second-harmonic distortion (SHD) of vertical-cavity surface-emitting lasers is investigated theoretically. Two parameters, differential confinement factor and differential cavity loss, are defined for the consideration of self-focusing and diffraction loss. It is found that SHD increases at low modulation frequencies due to the presence of differential cavity loss, especially for lasers with small core radius.

Index Terms—Lateral loss, second-harmonic distortion, semiconductor lasers modeling, small-signal modulation, vertical-cavity surface-emitting lasers.

I. INTRODUCTION

INTENSITY noise and chromatic fiber dispersion in analog optical communication systems are attributed to harmonic and intermodulation distortion in the amplitude modulation (AM) of semiconductor lasers. In addition, maximum usable bandwidth of the communication systems is limited by harmonic distortion [1], [2]. Therefore, devices with high linearity or small distortion, such as vertical cavity surface-emitting lasers (VCSEL) with stable single-mode operation, are highly desired. In fact, second-harmonic distortion (SHD) of VCSEL can be much lower than that of facet emitted devices due to its high relaxation oscillation frequency [3], since SHD is inversely proportional to the square of the relaxation oscillation frequency of lasers [4].

Nonlinearity such as gain compression, spontaneous emission and longitudinal spatial hole burning have been studied extensively on the induction of SHD in semiconductor lasers [3]. In general, SHD is induced in Fabry-Perot lasers by spontaneous emission and gain compression as well as spatial hole burning at modulation frequencies less than 0.1 GHz [2]. In particular, spontaneous emission has an influence on SHD at low bias (i.e., near threshold) but gain compression and spatial hole burning dominate at high bias level (i.e., 1.5 times threshold or above). Due to the use of Fabry Perot type resonator, similar dependency of SHD on these nonlinearities is expected in VCSEL. However, the modulation response of VCSEL may exhibit differently to that of facet emitted devices due to increased lateral losses because of its small core radius. In fact, it has been shown that lateral loss effects suppress self-sustained pulsation operation in VCSEL even with sufficient saturable absorption [5]. Therefore, lateral loss effects should

be taken into consideration in the analysis of the modulation response of VCSEL.

In this paper, the influence of lateral loss effects on the SHD of VCSEL is studied theoretically. Other nonlinearity such as spontaneous emission and spatial hole burning are ignored in the investigation as they are not of prime interest here. In Section II, the dependence of lateral loss effects on the carrier concentration under small-signal modulation is clarified. Differential confinement factor and differential cavity loss are defined in the calculation of lateral losses to take account of self-focusing and diffraction loss. In Section III, a simple rate-equation model of VCSEL is developed and SHD in the AM response of VCSEL is derived. Using this model, the values of confinement factor and cavity loss are extracted from the measured light/current curves of a fabricated VCSEL and a simulation is performed to investigate the influence of lateral loss effects on the SHD of the VCSEL. It is found that at low modulation frequencies, differential cavity loss has a much higher influence on SHD for devices with small core radius, while differential confinement factor has little effect. Brief discussion and conclusion are given in Section IV.

II. THEORETICAL PREDICTION OF LATERAL LOSS EFFECTS IN VCSEL

A. Confinement Factor and Differential Confinement Factor

Fig. 1 shows the phenomenon of self-focusing in VCSEL. The mechanism of self-focusing can be explained as the increase in focusing of the lateral field into the core region as the refractive index inside the active layer increases. In result the lateral optical confinement factor (Γ) of VCSEL is increased. For lasers under small signal modulation, the variation of refractive index inside the active layer is mainly due to the change of carrier concentration. Hence, the change of lateral confinement factor due to self-focusing is related to carrier concentration N and can be approximated by

$$\Gamma(N_s + \Delta N(t)) = \Gamma_s + \frac{\partial \Gamma}{\partial N} \Delta N(t) \quad (1)$$

where ΔN is the small change of carrier concentration, Γ_s and N_s are the lateral confinement factor and carrier concentration, respectively, at steady state. The parameter, $\partial \Gamma / \partial N$, is defined as the differential confinement factor which describes the modulation response of lateral confinement factor. It is shown in [6] that Γ_s decreases, but $|\partial \Gamma / \partial N|$ increases with the reduction of core radius. However, the sign of $\partial \Gamma / \partial N$ depends on the lateral optical confinement structure of lasers and

Manuscript received November 24, 1998; revised April 2, 1999. This work was supported by RGC Grant HKU7059/98E.

The authors are with the Department of Electrical and Electronic Engineering, University of Hong Kong, Pokfulam Road, Hong Kong.

Publisher Item Identifier S 1077-260X(99)05348-4.

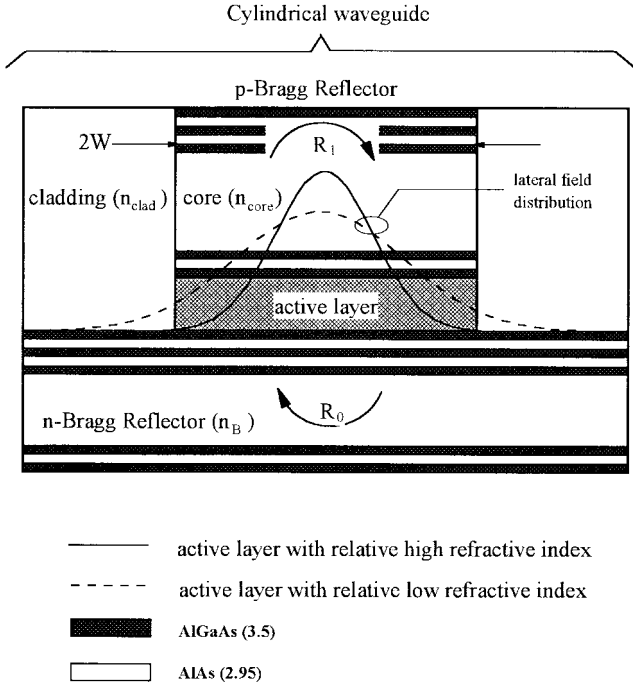


Fig. 1. Lateral distribution of optical field inside the active layer of a VCSEL. The solid line indicates that the focusing of lateral optical field into the core region due to the increase of refractive index inside the active layer.

$\partial\Gamma/\partial N$ has a negative value for VCSEL with index guiding structures.

B. Cavity Loss and Differential Cavity Loss

Fig. 2 shows the diffraction of light from a cylindrical waveguide into a Bragg reflector. The core radius of the device is W ; the refractive indices of core and cladding regions of the cylindrical waveguide are n_{core} and n_{clad} , respectively. The resultant angle of diffraction θ_2 , from the cylindrical waveguide (core and cladding) of effective refractive index n_{eff} into the Bragg reflector with effective refractive index n_B can be calculated from the theory of Fraunhofer diffraction and Snell's law of refraction [7]. Fig. 2(b) shows the angle of diffraction θ_1 as light leaves the core region of a circular aperture of radius W . From Fraunhofer diffraction theory

$$\theta_1 = \sin^{-1} \left(\frac{\lambda_o}{2W} \right) \quad (2)$$

where λ_o is the wavelength in the core region. Light is further refracted to θ_2 in the Bragg reflector. By Snell's law of refraction

$$n_{\text{eff}} \sin \theta_1 = n_B \sin \theta_2. \quad (3)$$

Substituting (3) into (2), θ_2 can be expressed as

$$\theta_2 = \sin^{-1} \left(\frac{\lambda_o n_{\text{eff}}}{2n_B W} \right). \quad (4)$$

Since the reflectivity R of a Bragg reflector is a function of θ_2 [8], (4) implies that R is dependent on n_{eff} . For the VCSEL shown in Fig. 1, the cavity loss α is given by

$$\alpha = \alpha_m + \frac{1}{L_{\text{eff}}} \log \left(\frac{1}{|R_0||R_1|} \right) \quad (5)$$

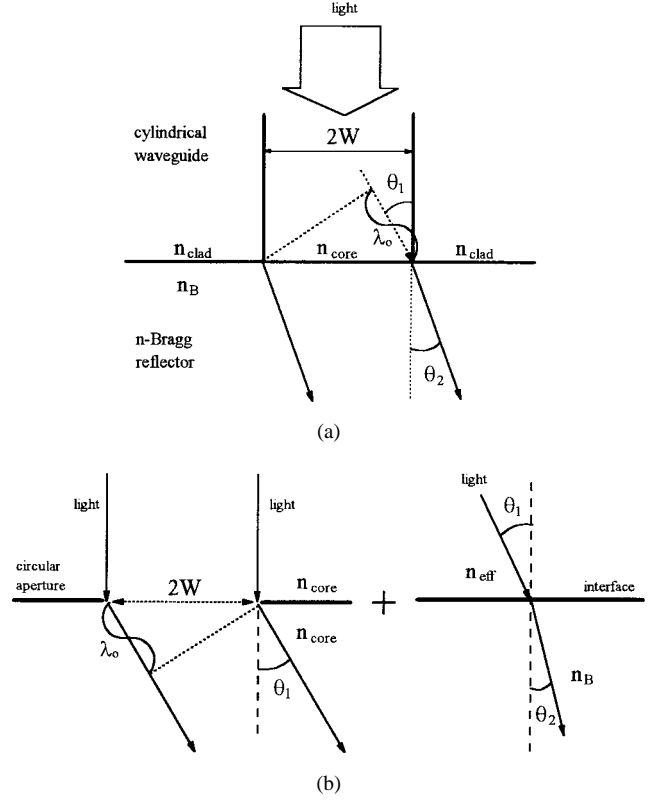


Fig. 2. The mechanism of light diffraction from a cylindrical waveguide. (a) Light diffraction through a circular aperture and refraction of light between two dielectric materials of refractive indices n_{eff} and n_B , respectively. (b) The explanation of light diffraction from a cylindrical waveguide using theory of Fraunhofer diffraction and Snell's Law of refraction.

where α_m is the material loss and L_{eff} is the effective cavity length. $|R_0|$ and $|R_1|$ are the field reflectivity of the n- and p-type Bragg reflectors, respectively. Hence, α is also dependent on n_{eff} as $|R_0|$ and $|R_1|$ are both functions of n_{eff} .

For devices under small signal modulation, any variation of α with small change of n_{eff} can be related to ΔN by

$$\alpha(N_s + \Delta N(t)) = \alpha_s + \frac{\partial \alpha}{\partial N} \Delta N(t) \quad (6)$$

where α_s is the total cavity loss at steady state and $\partial\alpha/\partial N$ is the differential cavity loss. The value of α_s can be deduced from the steady state value of $|R_0|$ and $|R_1|$ through (5). $\partial\alpha/\partial N$ can be obtained by differentiating (5) with respect to the carrier concentration, that is

$$\frac{\partial \alpha}{\partial N} = -\frac{1}{L_{\text{eff}}} \left(\frac{1}{|R_0|} \frac{\partial |R_0|}{\partial N} + \frac{1}{|R_1|} \frac{\partial |R_1|}{\partial N} \right) \quad (7)$$

where α_m and L_{eff} are assumed to be independent of the carrier concentration. $\partial|R_0|/\partial N$ and $\partial|R_1|/\partial N$ are the rate of change of $|R_0|$ and $|R_1|$ with respect to the carrier concentration, respectively. The value of $\partial\alpha/\partial N$ can thus be calculated from (7) provided that $|R_0|$ and $|R_1|$ are determined. The field reflectivity R_0 can be computed from [9]

$$R_0 \approx \int_0^\infty \frac{\beta_0 - H}{\beta_0 + H} \Phi_0 \Phi_0^* dk \quad (8)$$

where H is a transfer function of the Bragg reflector in k space, β_0 and Φ_0 are the propagation coefficients and the Hankel

transform of the fundamental lateral mode, respectively. It must be noted that H , β_0 , and Φ_0 are all dependent on n_{eff} . R_1 can be calculated using (8) in a similar manner.

It is expected that $|R_0|$ (as well as $|R_1|$) decreases with the reduction of W due to increased diffraction. Hence, the value of α_s increases with the reduction of W as α_s is inversely proportional to $|R_0|$. $|\partial\alpha/\partial N|$ would also increase with the reduction of W but the sign of $\partial\alpha/\partial N$ depends on the lateral optical confinement structure of VCSEL. For devices with index-guiding structure, $\partial\alpha/\partial N$ is negative. This can be shown by expressing (8) into a Fresnel reflectivity formula as given by [10]

$$|R_0| \approx \frac{n_B - n_{\text{eff}}}{n_B + n_{\text{eff}}}. \quad (9)$$

$|R_0|$ must be greater than zero and this implies $n_B > n_{\text{eff}}$. For devices with index guiding structure, the imaginary part of n_{eff} is negligible such that $\partial|R_0|/\partial N$ can be expressed as

$$\frac{\partial|R_0|}{\partial N} = \frac{-2n_B}{(n_B + n_{\text{eff}})^2} \frac{\partial n_{\text{eff}}}{\partial N} \quad (10)$$

where $\partial n_{\text{eff}}/\partial N$ ($\approx n_{\text{core}}/\partial N < 0$) is the effective change of refractive index with carrier concentration. From (10), $\partial|R_0|/\partial N$ is positive and this is also true for $\partial|R_1|/\partial N$. Alternatively, it can be shown that 1) $\partial|R_{0,1}|/\partial\theta_2$ is negative as $\theta_2 = 0$ is the global maximum of $|R_{0,1}|$ [8], and 2) $\partial\theta_2/\partial N$ is also negative as indicated in (4), thus $\partial|R_{0,1}|/\partial N = \partial|R_{0,1}|/\partial\theta_2 \times \partial\theta_2/\partial N$ is positive. Both of the above argument shows that $\partial\alpha/\partial N$ has a negative value for index guiding lasers. In the following paragraph, the magnitude and sign of Γ_s , $\partial\Gamma/\partial N$, α_s , and $\partial\alpha/\partial N$ are calculated for a VCSEL with index-guiding structure. We would attempt to see how these values vary in the VCSEL as we vary its core radius W , to verify if their relationships agree with predictions from our theoretical analysis presented here.

C. Calculation of Γ_s , $\partial\Gamma/\partial N$, α_s , and $\partial\alpha/\partial N$

The values of Γ_s , $\partial\Gamma/\partial N$, α_s , and $\partial\alpha/\partial N$ can be calculated for a schematic VCSEL given in Fig. 1. The device structure is similar to the fabricated VCSEL given in [11]. In our schematic VCSEL the top mirror is a p-type distributed Bragg reflector surrounded by a cladding layer of refractive index n_{clad} . The background effective refractive index of the core region (i.e., region including the top mirror and active layer) is equal to n_{core} . Since the entire top reflector is confined within the core region, light diffraction is negligible there and the reflectivity $|R_1|$ is assumed a constant. The bottom mirror is an n-type distributed Bragg reflector formed by alternate layers (26 pairs) of AlGaAs and AlAs with quarter wavelength thickness. The values of n_{clad} , n_{core} , $|R_1|$, and the refractive index distribution of the n-type Bragg reflector used in the calculation can be found in Table I.

Fig. 3 shows the variation of Γ_s , α_s , $\partial\Gamma/\partial N$, and $\partial\alpha/\partial N$ with core radius W . The value of Γ_s and $\partial\Gamma/\partial N$ are calculated [6] with the assumption that the small change of refractive index Δn inside the active layer is related to ΔN by

$$\Delta n = \frac{\partial n}{\partial N} \Delta N \quad (11)$$

TABLE I
PARAMETERS USED IN THE MODEL

Parameter	Symbol	Value
wavelength	λ_0	0.98 μm
group velocity	v_g	$0.83 \times 10^{10} \text{cm/s}$
longitudinal optical confinement factor	Γ_z	0.07
bimolecular carrier recombination coefficient	B_{sp}	$1 \times 10^{-10} \text{cm}^3 \text{s}^{-1}$
spontaneous emission factor	β	1×10^{-4}
active region thickness	d	0.1 μm
background refractive index in core region	n_{core}	3.45
background refractive index in cladding region	n_{clad}	3.43
carrier lifetime in active layer	τ_s	$3 \times 10^{-9} \text{s}$
carrier induced refractive index change	$\partial n/\partial N$	$-6.816 \times 10^{-21} \text{cm}^3$
gain suppression factor	ϵ	$1 \times 10^{-17} \text{cm}^3$
material loss	α_m	10cm^{-1}
effective cavity length	L_{eff}	0.7 μm
background temperature	T_r	300 $^\circ\text{K}$
thermal conductivity	κ	$0.45 \text{Wcm}^{-1}\text{C}^{-1}$
reflectivity of top Bragg reflector	$ R_1 $	0.997
characteristic temperature	T_0	30 $^\circ\text{K}$
refractive index of AlAs dielectric layer		2.95
refractive index of AlGaAs dielectric layer		3.5

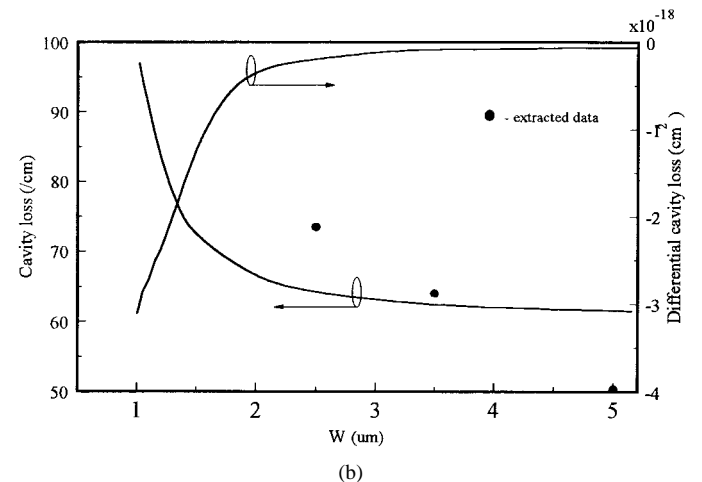
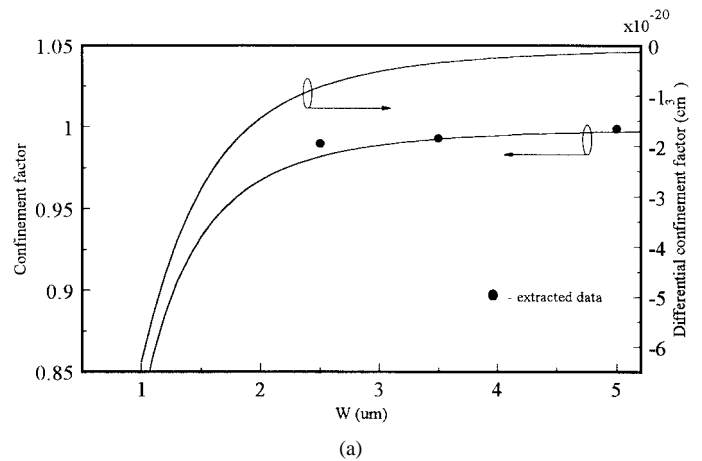


Fig. 3. (a) The variation of confinement factor (Γ_s) and differential confinement factor ($\partial\Gamma/\partial N$) with core radius, W . (b) The variation of cavity loss (α_s) and differential cavity loss ($\partial\alpha/\partial N$) with core radius, W .

where $\partial n/\partial N$ is the carrier induced index change. In addition, the values of α_s and $\partial\alpha/\partial N$ are calculated using (5) and (7) [5]. From the graphs of the calculated values in Fig. 3, it is clear that Γ_s , $\partial\Gamma/\partial N$, and $\partial\alpha/\partial N$ increase, but α_s decreases, with the increase of W . It can also be seen that both $\partial\Gamma/\partial N$ and $\partial\alpha/\partial N$ are negative for the whole range of W . As far as the general relationship between lateral loss parameters and core radius W is concerned, the calculated results for this VCSEL agree readily with the analytical prediction. In Section III, these relationships are further confirmed by data extracted from measured characteristic of the fabricated VCSEL given in [11].

III. MODULATION RESPONSE OF VCSEL WITH LATERAL LOSS EFFECTS

A. Rate-Equation Model with Lateral Loss Effects

Using a rate-equation model, values of Γ_s and α_s can be extracted from the measured light output versus current ($L-I$) curves of the fabricated VCSEL given in [11]. The rate-equation model has been applied to the VCSEL for other investigations with success [4] and is given by

$$\frac{\partial P(t)}{\partial t} = \nu_g(\Gamma(t)G(t) - \alpha(t))P(t) + \beta B_{sp}N^2(t) \quad (12)$$

$$\frac{\partial N(t)}{\partial t} = \frac{I(t)}{qV} - \nu_g\Gamma(t)G(t)P(t) - \frac{N(t)}{\tau_s} \quad (13)$$

$$C_{th}\frac{\partial T(t)}{\partial t} = (P_{IV}(t) - P_{hv}(t)) - \kappa\frac{T(t) - T_t}{R_{th}} \quad (14)$$

where P is the photon density, N is the carrier concentration and T is the effective temperature of laser cavity. In the photon rate equation, G is the equivalent modal gain, ν_g is the group velocity, β is the spontaneous emission factor and B_{sp} is the bimolecular carrier recombination factor. In the carrier rate equation, τ_s is the carrier lifetime, I is the injection current and V is the volume of the active layer. α and Γ given in (12) and (13) take into account α_s and Γ_s as well as $\partial\Gamma/\partial N$ and $\partial\alpha/\partial N$ for the consideration of lateral loss effects.

In the thermal rate equation, T_t is the temperature at threshold, κ is the thermal conductivity, R_{th} and C_{th} are the thermal resistance and capacitance, respectively, of the device. The output power P_{hv} of the device is given by

$$P_{hv} = \frac{1}{2}\nu_g h\nu(1 - |R_1|^2)\pi W^2\Gamma_z P \quad (15)$$

where h is the Planck's constant and ν is the frequency of the lasing mode. The total input electrical power P_{IV} is defined as

$$P_{IV} = V_F(N)I \quad (16)$$

where V_F is the voltage across the active layer and is given by [15]

$$V_F = \frac{1}{q}[E_g + k_B T \cdot \log\{(\exp(N/N_c) - 1) \cdot (\exp(N/N_v) - 1)\}] \quad (17)$$

where E_g ($= 1.519 - 5.408 \times 10^{-4} \times T^2/(T + 204)$) is the energy gap between the first quantized energy level of conduction and the valence bands of quantum wells active

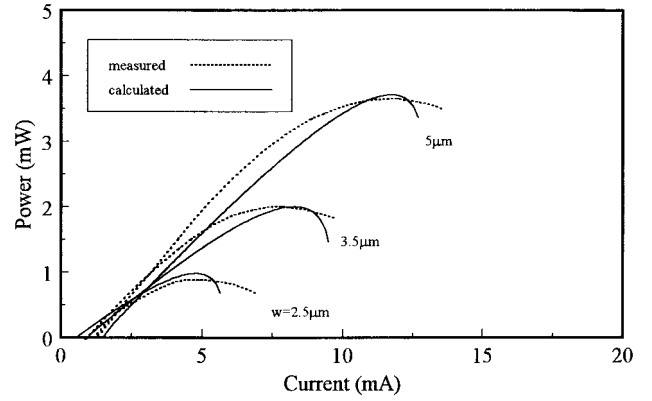


Fig. 4. Comparison of the measured and calculated light/current curves of VCSEL's with core radius equal to 2.5, 3.5, and 5 μm .

layer and k_B is the Boltzmann constant. N_c and N_v are the effective conduction and valence edge density of states, respectively, and can be expressed as

$$N_{c/v} = m_{c/h}^* k_B T / \pi \hbar^2 L_z \quad (18)$$

where $\hbar = h/2\pi$, $m_{c/h}^*$ ($= 0.0665/0.33196$) is the effective mass of electron/holes and L_z ($= 80 \text{ \AA}$) is the thickness of quantum wells.

The influence of nonlinear gain is considered in the model through the carrier and photon dependence of G that is defined as

$$G = \frac{G_0}{1 + \varepsilon P} \quad (19)$$

where ε is the gain compression factor. G_0 is the unsaturated optical gain that is only dependent on the carrier concentration and can be expressed as

$$G_0 = \Gamma_z a_N \log(N/N_0) \quad (20)$$

where Γ_z is the longitudinal confinement factor, a_N is the gain parameter and N_0 is the carrier concentration at transparency. In (20), the parameters, a_N and N_0 , are assumed to vary with temperature and their dependence are approximated by $a_N = -46963.3 + 371.56 \times T - 0.941029 \times T^2 + 7.99274 \times 10^{-4} \times T^3$, $N_0 = (2.723 - 0.02417 \times T + 6.4786 \times 10^{-5} \times T^2) \times 10^{18}$ and N in G_0 is normalized by $0.41 \times 10^{18} \text{ cm}^{-3}$. The temperature dependence of the threshold current density J_{th} (at 300 K) is described by the Arrhenius-type relation [12]

$$J_{th}(T) = J_o \exp\left(\frac{T - 300}{T_o}\right) \quad (21)$$

where J_o is the threshold current density at 300 K and T_o is the characteristic temperature. J_o can be expressed as $J_o = qdN_{th}/\tau_s$ where N_{th} is the threshold carrier concentration at 300 K and d is the thickness of the active layer.

Fig. 4 shows the measured [11] and calculated light/current curves of the fabricated VCSEL at different W . The calculated data are obtained from (12)–(14) using (15)–(21) as the auxiliary equations. In the calculation, $\partial P/\partial t$ and $\partial N/\partial t$ and $\partial T/\partial t$ as well as $\partial\Gamma/\partial N$ and $\partial\alpha/\partial N$ are set to zero, P , N , and T are then solved in a self-consistent manner. By matching the measured light/current curves given in [11] with

TABLE II
SIZE DEPENDENCE OF OPTICAL LOSS AND THERMAL RESISTANCE OF VCSEL'S

core radius W (μm)	lateral confinement Γ_s	optical loss α_s (cm^{-1})	Thermal Resistance R_{th} (cm^{-1})
2.5	0.990	73	7100
3.5	0.993	64	4200
5	0.999	50.3	2900

the calculated curve, the values of Γ_s , α_s , and R_{th} used in the model are extracted from the experimental data. Extracted values of Γ_s , α_s , and R_{th} are listed in Table II and other laser parameters used in the rate-equation model are given in Table I. The values of Γ_s and α_s are also plotted in Fig. 3 (indicated as solid circle) for comparison with the calculated data from the VCSEL in Fig. 1. As we can see, Γ_s and α_s extracted from the index-guided VCSEL in [11] exhibit precisely the same kind of variation with W as would have predicted by the calculated results from the similar structured VCSEL in Section II above.

B. Small-Signal Modulation Response of VCSEL: Second-Harmonic Distortion

The rate-equation model can be simplified into two differential equations by using the quasistatic steady approximation on T [4]. It is noted that the thermal lifetime of lasers is much longer than the oscillation period of N and P . Therefore, the time derivative term in (14) can be ignored and the corresponding auxiliary thermal equation for quasi-steady state temperature T_s is given by

$$T_s = R_{\text{th}} \cdot (P_{\text{IV}} - P_{\text{hv}}) / \kappa + T_t. \quad (22)$$

The small signal modulation response of VCSEL can be obtained by perturbation method [6]. This can be done by equating I , N , and P with

$$I(t) = I_s + \Delta I(t) = I_s + I_1 e^{j\omega t} \quad (23a)$$

$$N(t) = N_s + \Delta N(t) = N_s + N_1 e^{j\omega t} + N_2 e^{j2\omega t} \quad (23b)$$

$$P(t) = P_s + \Delta P(t) = P_s + P_1 e^{j\omega t} + P_2 e^{j2\omega t} \quad (23c)$$

where $j = \sqrt{-1}$, I_s is the bias current, I_1 and ω are the amplitude and modulation frequencies of the sinusoidal modulation current, respectively. The subscript s stands for the steady state. By substituting (23a)–(23c) into the rate equations (12) and (13), and after some manipulations, the AM response and SHD of VCSEL with lateral loss effects are given by

$$\frac{P_1}{I_1} = \frac{\frac{\nu_g P_s}{qV} \Gamma_s \frac{\partial G_{\text{eff}}}{\partial N}}{(\omega_f^2 - \omega^2) + j\omega \nu_g \left(\kappa_s - \Gamma_s \frac{\partial G}{\partial P} P \right)} \quad (24)$$

$$\frac{P_2}{P_1} = \frac{(2j\omega + \nu_g \kappa_s) F(\omega) - \nu_g P_s \Gamma_s \frac{\partial G_{\text{eff}}}{\partial N} E(\omega)}{(\omega_f^2 - 4\omega^2) + 2j\omega \nu_g \left(\kappa_s - \Gamma_s \frac{\partial G}{\partial P} P_s \right)} P_1. \quad (25)$$

The relaxation oscillation frequency ω_f is defined as

$$\omega_f^2 = \nu_g^2 \Gamma_s \left(\alpha_{\text{eff}} \frac{\partial G_{\text{eff}}}{\partial N} - \kappa_s \frac{\partial G}{\partial P} \right) P_s \quad (26)$$

where

$$\frac{\partial G_{\text{eff}}}{\partial N} = \frac{\partial G}{\partial N} + \frac{1}{\Gamma_s} \left(G_s \frac{\partial \Gamma}{\partial N} - \frac{\partial \alpha}{\partial N} \right)$$

$$\alpha_{\text{eff}} = \alpha_s \left(1 - \frac{\varepsilon P_s}{1 + \varepsilon P_s} \right)$$

$$\kappa_s = \frac{1}{\nu_g \tau_s} + \left(G_s \frac{\partial \Gamma}{\partial N} + \Gamma_s \frac{\partial G}{\partial N} \right) P_s$$

$$\frac{\partial G}{\partial P} = -\frac{\varepsilon \alpha}{\Gamma_s (1 + \varepsilon P_s)} \quad \text{and} \quad \frac{\partial G}{\partial N} \frac{\Gamma_z a_N}{N_0} \exp \left\{ -\frac{\alpha_s}{\Gamma_s \Gamma_z a_N} \right\}.$$

In (25), $F(\omega)$ and $E(\omega)$ are defined as

$$E(\omega) = \nu_g P_s \frac{\partial \Gamma}{\partial N} K(\omega) \left[\frac{\partial G}{\partial P} + \frac{\partial G}{\partial N} K(\omega) \right] + \nu_g \Gamma_s \left[\frac{\partial G}{\partial P} + \left(\frac{\partial G_{\text{eff}}}{\partial N} + \frac{1}{\Gamma_s} \frac{\partial \alpha}{\partial N} \right) K(\omega) \right] \quad (27a)$$

$$F(\omega) = \nu_g P_s \frac{\partial \Gamma}{\partial N} K(\omega) \left[\frac{\partial G}{\partial P} + \frac{\partial G}{\partial N} K(\omega) \right] + \nu_g \Gamma_s \left[\frac{\partial G}{\partial P} + \frac{\partial G_{\text{eff}}}{\partial N} K(\omega) \right] \quad (27b)$$

where

$$K(\omega) = \left(\nu_g P_s \Gamma_s \frac{\partial G_{\text{eff}}}{\partial N} \right)^{-1} \times \left(j\omega - \nu_g \Gamma_s P_s \frac{\partial G}{\partial P} \right).$$

As we can see, $E(\omega)$ and $F(\omega)$ are only different by an extra term, $\nu_g (\partial \alpha / \partial N) K(\omega)$. In the above derivation, we have ignored spontaneous emission term.

Fig. 5 shows the SHD of the fabricated VCSEL, calculated from (25), at $W = 3.5$ and $W = 5 \mu\text{m}$. The device is biased at around $I_s = 4$ mA with steady state output power of 1 mW and undergoes small signal current modulation (~ 0.5 mA) of frequency ω . In the calculations, the values of Γ_s , α_s , and R_{th} are obtained from Table II. At each W value, two curves are obtained. In the first, both $\partial \Gamma / \partial N$ and $\partial \alpha / \partial N$ are set to zero to simulate the SHD response without lateral loss effects. In the second, $\partial \Gamma / \partial N$ and $\partial \alpha / \partial N$ are assigned their most probable values (At $W = 3.5 \mu\text{m}$, $\partial \Gamma / \partial N$ and $\partial \alpha / \partial N$ are equal to $-0.4 \times 10^{-20} \text{ cm}^3$ and $-0.1 \times 10^{-18} \text{ cm}^2$. At $W = 5 \mu\text{m}$, $\partial \Gamma / \partial N$ and $\partial \alpha / \partial N$ are equal to $-0.02 \times 10^{-20} \text{ cm}^3$ and $-0.03 \times 10^{-18} \text{ cm}^2$) according to Fig. 3 to simulate the response with lateral loss. In the figure, the dotted and dashed lines represent the VCSEL SHD with and without lateral loss effects, respectively. It is observed that, at low modulation frequencies, SHD with lateral loss effects is much higher than that without lateral loss. For modulation frequencies below a cutoff frequency ω_{cutoff} (e.g., $\omega < 0.6 \times 10^8 \text{ Hz} = \omega_{\text{cutoff}}$ for the device with $W = 3.5 \mu\text{m}$), SHD is very much independent of ω . For modulation above

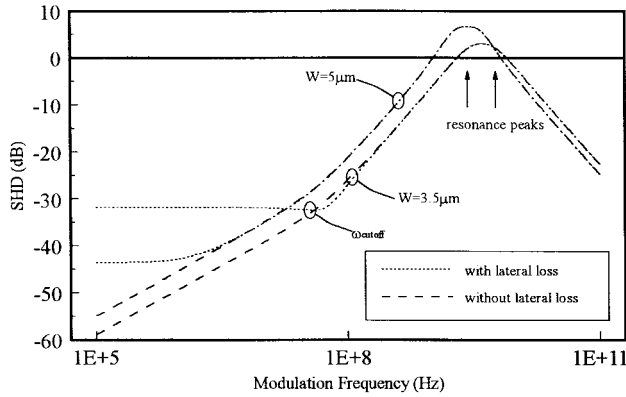


Fig. 5. Second-harmonic distortion of VCSEL's with core radius of 3.5 and 5 μm . The steady-state output power of VCSEL's is set to 1 mW.

the cutoff, $\partial\Gamma/\partial N$ and $\partial\alpha/\partial N$ have little effect on SHD as the SHD curves with and without lateral loss essentially overlap. Furthermore, When core radius W is increased from 3.5 to 5 μm , at no lateral loss, SHD is uniformly increased throughout all modulation frequencies up to ω_f ; in the more realistic situation where lateral loss is present, the SHD is decreased, and the cutoff frequency is lowered resulting in a narrower modulation bandwidth.

From the above numerical analysis, it is clear that the two lateral loss parameters, either $\partial\Gamma/\partial N$ or $\partial\alpha/\partial N$, or both, have profound effect on SHD only at low modulation frequencies. It is interesting then to further investigate how each of the lateral loss parameter affects the SHD. This can be done analytically by simplifying the expression for SHD in (25) at low modulation frequencies. Hence, for $\omega \ll \omega_f$, (24) and (25) is reduced to

$$\frac{P_1}{I_1} \approx \frac{\nu_g P_s \Gamma_s \frac{\partial G_{\text{eff}}}{\partial N}}{qV \omega_f^2} \quad (28)$$

$$\frac{P_2}{P_1} \approx \frac{\nu_g \kappa_s F(\omega) - \nu_g P_s \Gamma_s \frac{\partial G_{\text{eff}}}{\partial N} E(\omega)}{\omega_f^2} P_1. \quad (29)$$

For large P_s (say $5 \times 10^{15} \text{ cm}^{-3}$), the value $\Gamma_s (\partial G/\partial N) P_s$ of is roughly equal to 0.25 cm^{-1} which is larger than $1/\nu_g \tau_s (= 0.04 \text{ cm}^{-1})$. Thus $(1/\nu_g \tau_s) + P_s G_s (\partial G_{\text{eff}}/\partial N) \ll P_s \Gamma_s (\partial G/\partial N)$, therefore, $\kappa_s \approx P_s \Gamma_s (\partial G_{\text{eff}}/\partial N)$. The numerator of (29) becomes $\nu_g P_s \Gamma_s (\partial G_{\text{eff}}/\partial N) \cdot \nu_g (\partial\alpha/\partial N) K(\omega)$ where $K(\omega) \approx (\partial G/\partial P) (\partial G_{\text{eff}}/\partial N)^{-1}$ at low modulation frequencies. Equation (29) can then be reduced to

$$\frac{P_2}{P_1} \approx \nu_g P_s \Gamma_s \cdot \nu_g \frac{\partial\alpha}{\partial N} \frac{\partial G}{\partial P} \frac{P_1}{\omega_f^2}. \quad (30)$$

Thus the expression for SHD is reduced to a form independent of ω conforming to the leveling SHD region in Fig. 5 for modulation frequencies below ω_{cutoff} . From (24) and (26), P_1 and ω_f are related to $\partial\Gamma/\partial N$ and $\partial\alpha/\partial N$ through $(\partial G_{\text{eff}}/\partial N) = (\partial G/\partial N) + (1/\Gamma_s) (G_s (\partial\Gamma/\partial N) - (\partial\alpha/\partial N))$. In a typical VCSEL, the true values of $G_s \partial\Gamma/\partial N$ and $\partial\alpha/\partial N$ (see Fig. 3) are 100 times less than $\partial G/\partial N$ such

that $(\partial G_{\text{eff}}/\partial N) \approx (\partial G/\partial N)$, indicating that P_1 and ω_f are essentially independent of $\partial\Gamma/\partial N$ and $\partial\alpha/\partial N$. The term $(\partial G/\partial P) = -(\epsilon\alpha_s/\Gamma_s(1 + \epsilon P_s))$ does not involve $\partial\Gamma/\partial N$ and $\partial\alpha/\partial N$. Thus (30) describes that SHD is directly proportional to $|\partial\alpha/\partial N|$ at low modulation frequencies. $\partial\Gamma/\partial N$ has no effect here.

IV. DISCUSSION AND CONCLUSION

From the above, the effect of lateral loss on SHD due to differential cavity loss $\partial\alpha/\partial N$ kicks in at modulation frequencies below ω_{cutoff} (e.g., 600 MHz in the device with $W = 3.5 \mu\text{m}$). This is a source of noise in optical systems. A common approach used for transmitting signal is by intensity modulation and two major problems exist in such a scheme: the noise levels produced are high and the full bandwidth of the optical system cannot be used [13]. In Fig. 5, the device at $W = 5 \mu\text{m}$ exhibits about -45 dB SHD, and the device at $W = 3.5 \mu\text{m}$ exhibits a little over -30 dB SHD. Such levels of intensity noise are pretty much in line with those that are found in edge emitting devices [14]. However, VCSEL allows for a much larger modulation bandwidth. Our study show that paying careful consideration to lateral loss effects coupled with smaller core size design, the VCSEL devices can offer more promising solution than edge emitting laser device to the problems that exist in the intensity modulation systems. As observed in our simulation, using a larger core radius W reduces SHD, but in the expense of modulation bandwidth, since the cutoff frequency ω_{cutoff} would be lowered. The increase in SHD at smaller W is due to a combination of increase in Γ_s, α_s , and $\partial\alpha/\partial N$ as W decreases. Thus, it becomes more critical to consider lateral loss effects and means of minimizing SHD, when designing VCSEL with small core size. For example, it can be observed from (30) that the dependence of SHD on $\partial\alpha/\partial N$ can be reduced by decreasing $\partial G/\partial P$, via the reduction of gain compression factor ϵ . Furthermore, the direct relationship between SHD and $\partial\alpha/\partial N$ in (30) assumes that the photon density P_s is large. Lowering the output intensity can, therefore, also reduce the dependence of SHD on $\partial\alpha/\partial N$.

In conclusion, the influence of lateral loss effects on the SHD of VCSEL is investigated theoretically. Two parameters, $\partial\Gamma/\partial N$ and $\partial\alpha/\partial N$, are defined for the consideration of self-focusing and diffraction loss in VCSEL under small signal modulation. A simple rate-equation model is developed and the analytical expression of SHD is derived. It is shown that $|\partial\alpha/\partial N|$ is the dominant factor that induces SHD at low modulation frequencies, especially for devices with small core radius.

REFERENCES

- [1] T. E. Darcie and R. S. Tucker, "Intermodulation and harmonic distortion in InGaAsP lasers," *Electron. Lett.*, vol. 21, pp. 665–666, 1985.
- [2] G. Morthier, F. Libbrecht, K. David, P. Vankwikelberge, and G. Baets, "Theoretical investigation of the second order harmonic distortion in the AM response of 1.55 μm F-P and DFB lasers," *IEEE J. Quantum Electron.*, vol. 27, pp. 1990–2002, Aug. 1991.
- [3] D. Tauber, G. Wang, R. S. Geels, J.E. Bowers, and L. A. Coldern, "Large and small signal dynamics of vertical cavity surface emitting lasers," *Appl. Phys. Lett.*, vol. 62, pp. 325–327, 1993.

- [4] S. F. Yu, W. N. Wong, P. Shum, and E. H. Li, "Theoretical analysis of modulation response and second harmonic distortion in vertical cavity surface emitting lasers," *IEEE J. Quantum Electron.*, vol. 32, pp. 2139–2147, Dec. 1996.
- [5] S. F. Yu and E. H. Li, "Influence of lateral field on the relaxation oscillation frequency of semiconductor lasers," *IEEE J. Quantum Electron.*, vol. 32, pp. 1–3, Jan. 1996.
- [6] S. F. Yu, "Analysis and design of vertical cavity surface emitting lasers for self-sustained pulsation operation," *IEEE J. Quantum Electron.*, vol. 34, pp. 497–505, Mar. 1998.
- [7] E. Hechit, *Optics*, 2nd ed., Addison-Wesley, 1987.
- [8] Y. Yeh, *Optical Waves in Layered Media*. New York: Wiley, 1988, ch. 6.
- [9] R. R. Burton, M. S. Stern, P. C. Kendall, and P. N. Robson, "Modeling of diffraction in pillar vertical cavity surface emitting lasers with embedded Bragg layers," *Opt. Quantum Electron.*, vol. 28, pp. 1677–1684, 1996.
- [10] J. K. Butler and J. Zoroofchi, "Radiation fields of GaAs-(AlGa)As Injection lasers," *IEEE J. Quantum Electron.*, vol. pp. 809–815, 1974.
- [11] J. W. Scott, R. S. Geels, S. W. Corzine, and L. A. Coldren, "Modeling temperature effects and spatial hole burning to optimize vertical cavity surface emitting laser performance," *IEEE J. Quantum Electron.*, vol. 29, pp. 1295–1308, 1993.
- [12] N. K. Dutta, J. Lopata, D. L. Sivco, and A. Y. Cho, "Temperature dependence of threshold of strained quantum well lasers," *Appl. Phys. Lett.*, vol. 58, no. 11, pp. 1125–1127, 1991.
- [13] J. Singh, *Optoelectronics—An Introduction to Materials and Devices*. New York: McGraw Hill, 1996, ch. 10.
- [14] G. Keiser, *Optical Fiber Communications*. New York: McGraw Hill, 1991, ch. 4.
- [15] R. S. Zory, Ed., *Quantum Well Lasers*. New York: Academic, 1993, ch. 1.

P. C. Chui, photograph and biography not available at the time of publication.



S.-F. Yu received the degree of B.E. (first class Honors) degree in electronic engineering from London University, University College, U.K., in 1990 and the degree of Doctor of Philosophy in optoelectronics engineering from Cambridge University, Robinson College, U.K., in 1993.

He joined the Department of Electronic Engineering, Sha Tin Technical Institute, Hong Kong, as a part-time Lecturer in 1993. In 1994, he joined the Department of Electrical and Electronic Engineering, the University of Hong Kong, where he was a Lecturer. Since 1996, he has been an Assistant Professor in the same department of the University of Hong Kong. His main research interest includes the fundamental study, optimization and the practical applications of semiconductor lasers. He currently conducts the development of high performance semiconductor lasers using diffused quantum-well materials for the application in long haul optical fiber communication systems. Furthermore, he involves in the development of novel mid-infrared vertical cavity lasers using quantum cascade architecture and their applications in the measurement of gas and liquid concentrations. He also studies the possibilities of using organic materials to fabricate integrated optoelectronics circuit including lasers, modulators and photodetectors for the industrial applications. He has published over 70 international technical papers including invited conference and journal papers as well as two book chapters.

Dr. Yu was awarded the traditional Departmental Prize by the Department of Electronics and Electrical Engineering, University College London in the final year degree examination. He was a Fellow and Honorary Scholar of Cambridge Commonwealth Trust Society. He also held a Croucher Foundation scholarship and an overseas research student award while studying for the doctoral program. Dr. Yu is a member of the SPIE. He is also in the executive committee, and is the seminar program chair of the seminar and meeting committee of SPIE Hong Kong Chapter. His biography has published in *Who's Who In Science And Engineering* (4th ed., Marquis), *Dictionary of International Biography* (25th ed.), and the *International Directory of Distinguished Leadership* (17th ed.).